Received: 30 June 2021 | Revised: 19 December 2021 | Accepted: 7 February 2022

DOI: 10.1002/jsp2.1195

SPECIAL ISSUE ARTICLE

JOR Spine OPEN ACCESS

Focal osteoporosis defect is associated with vertebral compression fracture prevalence in a bone mineral density-independent manner

Chentian Li[1,2] | Chi Ma[2] | Xianglong Zhuo[3] | Li Li[2,3] | Bing Li[3] | Songjian Li[1] | William W. Lu[2,4]

[1]Department of Orthopedics and Taumatology, Zhujiang Hospital, Southern Medical University, Guangzhou, Guangdong, China

[2]Department of Orthopaedics & Traumatology, Li Ka Shing Faculty of Medicine, The University of Hong Kong, Hong Kong SAR, China

[3]Department of Orthopaedics, Liuzhou Worker's Hospital, Guangxi Medical University, Liuzhou, Guangxi, China

[4]SIAT & Shenzhen Institutes of Advanced Technology, Chinese Academy of Science, Shenzhen, Guangdong, China

Correspondence
Songjian Li, Department of Orthopedics and Taumatology, Zhujiang Hospital, Southern Medical University, Guangzhou, Guangdong, China.
Email: lisongjian321@126.com

William W. Lu, Department of Orthopaedics & Traumatology, The University of Hong Kong, Hong Kong SAR, China.
Email: wwlu@hku.hk

Funding information
Shenzhen Significant Strategy Layout Project, Grant/Award Number: JCYJ 20170413162104773

Abstract

Introduction: Focal osteoporosis defect has shown a high association with the bone fragility and osteoporotic fracture prevalence. However, no routine computed tomography (CT)-based vertebral focal osteoporosis defect measurement and its association with vertebral compression fracture (VCF) were discussed yet. This study aimed to develop a routine CT-based measurement method for focal osteoporosis defect quantification, and to assess its association with the VCF prevalence.

Materials and Methods: A total of 205 cases who underwent routine CT scanning, were retrospectively reviewed and enrolled into either the VCF or the control group. The *focal bone mineral content loss (focal BMC loss)*, measured as the cumulated demineralization within bone void space, was proposed for focal osteoporosis defect quantification. Its scan-rescan reproducibility and its correlation with trabecular bone mineral density (BMD) and apparent microarchitecture parameters were evaluated. The association between *focal BMC loss* and the prevalence of VCF was studied by logistic regression.

Results: The measurement of *focal BMC loss* showed high reproducibility (RMSSD = 0.011 mm, LSC = 0.030 mm, ICC = 0.97), and good correlation with focal bone volume fraction ($r = 0.79$, $P < 0.001$), trabecular bone separation ($r = 0.76$, $P < 0.001$), but poor correlation with trabecular BMD ($r = 0.37$, $P < 0.001$). The *focal BMC loss* was significantly higher in the fracture group than the control (1.03 ± 0.13 vs. 0.93 ± 0.11 mm; $P < 0.001$), and was associated with prevalent VCF (1.87, 95% CI = 1.31–2.65, $P < 0.001$) independent of trabecular BMD level.

Discussion: As a surrogate measure of focal osteoporosis defect, *focal BMC Loss* independently associated with the VCF prevalence. It suggests that focal osteoporosis defect is a common manifestation that positively contributed to compression fracture risk and can be quantified with routine CT using *focal BMC Loss*.

Chentian Li, Chi Ma, and Xianglong Zhuo were contributed equally to this work.

KEYWORDS
deformity, degeneration, imaging, structure function relationships

1 | INTRODUCTION

Bone mineral density (BMD) measurements are widely used for the diagnosis of osteoporosis. Nevertheless, the BMD measurements alone have limited ability for fracture prediction.[1] Eighty-two percent of postmenopausal women with fracture had integral BMD level higher than the osteoporosis criterion.[2] Recent studies further demonstrated that the focal osteoporosis ("focal regions of larger trabecular defects"[3]), instead of the total bone density, have better ability for the osteoporotic fractures discrimination.[3,4] More studies showed that the subregional loss of BMD and structural integrity positively contributed to bone fragility.[5–7] Evidence suggests the focal osteoporosis defects, besides the average loss of bone density, is an additional risk factor associated with the osteoporotic fracture.

Although the average BMD measurements using routine computed tomography (CT) images is of considerable interest,[8] fewer studies on the focal osteoporosis changes in the vertebral bones were reported. Previous studies that measured the localized microarchitecture changes required dedicated high-resolution scans,[9–12] and not available for focal osteoporosis defect evaluation in clinical practice. Other clinical CT-based research[3,4,6] only focused on the spatial distribution of localized bone density, while merely evaluated the actual size of focal osteoporosis defects. The routine CT-based methods for focal osteoporosis defect evaluation were not thoroughly investigated yet, and the association of focal osteoporosis defect with the prevalence of vertebral fractures was poorly understood.

This study aimed to develop and validate a novel measure for focal osteoporosis defect evaluation in routine CT images, and to investigate the association of focal osteoporosis defect with the prevalence of vertebral compression fractures (VCFs).

2 | MATERIALS AND METHODS

2.1 | Study population

This study was performed as an ancillary study of osteoporosis research performed from 2015 to 2020 by local hospitals using the retrospective CT image datasets (Approval No. KY2020237). CT datasets of patients over 50 years old were respectively reviewed, and patients with VCF (Genant Grade ≥ 1[13]) at any level were recruited to the VCF group, while those with no VCF (Genant Grade $= 0$) were recruited to the control group, matched by age and sex. Cases were excluded if they had metabolic diseases, cancer, metastasis, or other spinal disorders (spine sclerosis and intervertebral disc hernias). As the L1 vertebral body was present in the largest proportion of study participants, only the scans with intact L1 vertebrae were selected. Thus, only the patients without L1 level fracture were included. Finally, 91 fracture cases and 114 control cases were included.

2.2 | CT image scanning protocol

The enrolled datasets were initially scanned in spinal view, using Siemens Somatom Definition Flash CT scanner (Siemens) at 120 kVp, with the automatic tube current mode and 1 mm scanning thickness. Images were routinely reconstructed using B30s kernel with a 0.7 mm slice increment, and a reconstruction field of view of 20 cm, leading to an in-plane spatial resolution of 0.4×0.4 mm.

2.3 | Image analysis

2.3.1 | Region of interests segmentation and image alignment

The L1 vertebral body regions were semi-automatically masked using the Growcut module,[14] and the central axis of the vertebral column was manually aligned to the z-axis orientation in Slicer (v4.8.1, http://www.slicer.org[15]). The final region of interest was determined by 6 mm distance erosion from the mask, to ensure the cortical regions were removed (Figure 1A). After segmentation, BMD and focal osteoporosis measurements were automatically performed using an in-house python software following the steps below.

2.3.2 | Asynchronous BMD measurement

The BMD was measured using an asynchronous calibration method.[16] In brief, the calibration equation was determined by the linear correlation equation between the measured CT value and the known hydroxyapatite-calcium equivalent density of the phantom inserts (Syngo Osteo, Siemens) from five datasets with same scanning protocol. Subsequently, the CT-attenuation values in all datasets were calibrated to the BMD based on the calibration equation. The trabecular BMD was determined by average density in the vertebral region of interest (ROI).

2.3.3 | Focal osteoporosis defect evaluation

Image normalization

The images were resized to $0.3 \times 0.3 \times 0.3$ mm^3 using a linear interpolation method. Then an unsharp masking filtering[17,18] was performed to enhance the signal-to-noise ratio. In brief, Gaussian filtering

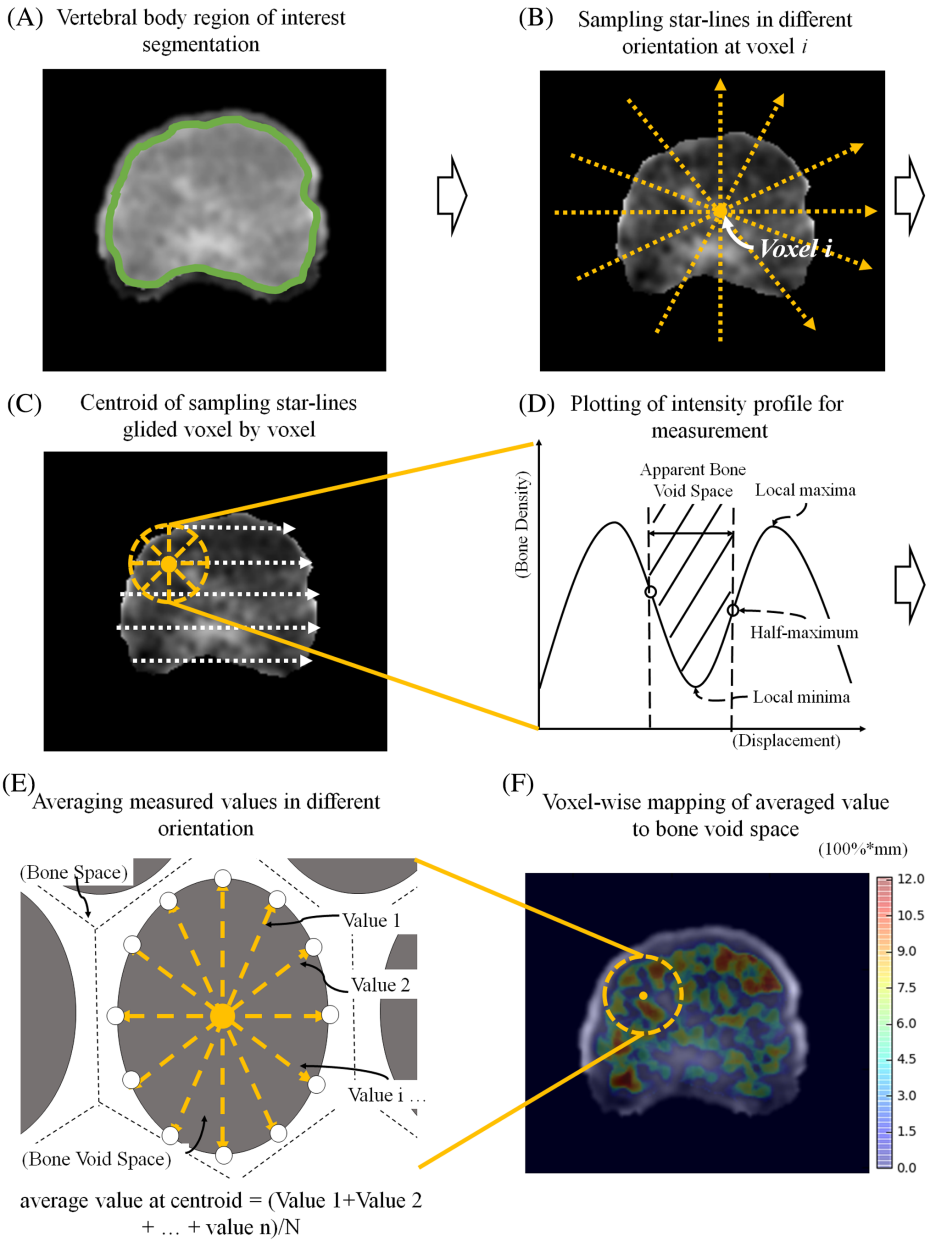

FIGURE 1 Summary of focal osteoporosis defect measurement approach. (A) Manually segmentation of the vertebral body ROI. (B) The intensity profiles were sampled along the differently orientated star-lines. (C) The centroid of the star-lines was glided voxel by voxel along with the white arrows, and the star-lines were running through the whole ROI (the orange circle represented a field of view that zoomed up in panel D). (D) The focal osteoporosis defect-related measurements were performed for each intensity profile. (E) Measured value from different star-lines at one centroid was averaged. (F) The averaged value at the centroid was mapped to the corresponding voxel in the vertebral body image)

with a sigma of 0.3 mm was applied to the resized image to reduce the high-frequency noises.

Starline-based intensity profile tracing

The intensity profiles of the cross-sectional image were first sampled in different orientations, based on a star-line tracing strategy.[19] The sampling lines were rotated with an optimized angle of 12° to obtain differently orientated profiles (Figure 1B). The centroid of the sampling star-lines was glided voxel-by-voxel within the ROI (Figure 1C). The star-lines were running through the whole ROI, and this step repeated for every voxel in the ROI in a one-by-one fashion.

Apparent focal bone void space identification

Following intensity profile sampling, the full width at half-maximum measurement strategy[20,21] was adopted to identify the apparent bone void space. Briefly, the ridges and valleys in the intensity profile were located by finding the localized maxima and minima, the localized region with intensity less than 0.5 × (maxima + minima) was defined as the bone void space. Intuitively, apparent focal bone void spaces are the valleys of intensity profiles (Figure 1D).

Definitions of the focal osteoporosis defect *measurements*

Several correlated measurements were defined to quantify the focal osteoporosis defect:

(i) Intercept Width (IncptWidth): Defined as the length of the bone void space calculated as:

$$IncptWidth = P_{(i+1)} - P_{(i)}\ (mm) \quad (1)$$

where i is the ith voxel in the ROI, $P_{(i)}$ is the start point of bone void space, and $P_{(i+1)}$ is the endpoint of this space.

(ii) Focal bone mineral density loss (focal BMD loss): To measure the focal BMD loss, the voxel-wise BMD loss percentage from 1200 mg/cm^3 was calculated first. Following the assumption by a previous study,[22] the voxel-wise BMD percentage loss at each voxel was calculated as:

$$BMD_{loss\,i} = \frac{1200 - BMD_i}{1200}(100\%) \quad (2)$$

where BMD_{lossi} is the amount of bone density loss at the voxel i in the intensity profile, and 1200 mg/cm^3 is the reference density of the assumed intact bone tissue. Intuitively, this value presented the percentage of BMD loss compared to the reference intact bone tissue density level.

Subsequently, the *focal bone mineral density loss* (focal BMD loss) of the focal bone void space was defined as:

$$Focal\,BMD\,loss = \frac{\sum_{i=0}^{IncptWidth} BMD_{loss\ i}}{IncptWidth}(100\%) \quad (3)$$

where *IncptWidth* is the width of the bone void space. Intuitively, the focal BMD loss is the density gap between the case and the assumed intact bone tissue that needs to be filled in the focal void space.

(iii) Focal bone mineral content loss (focal BMC loss): Defined as the cumulated bone density loss percentage from 1200 mg/cm^3 in the bone void space. The equation for the computation could be represented as:

$$Focal\,BMC\,loss = focal\,BMD\,loss * IncptWidth\,(mm) \quad (4)$$

where *focal BMD loss* is the focal bone density loss in the bone void space, and *IncptWidth* is the Intercept Width (*focal BMC loss* is the area above the curve shown in Figure 1D).

Voxel-wise parameter mapping and average value calculation

As there were multiple orientated intensity profiles for one voxel, the measured values in different orientation were averaged (Figure 1E) and mapped to the corresponding voxel location (Figures 1F and 2). Finally, the mapped values in one vertebra ROI were averaged to represent the overall status of the case. In our experiments under the

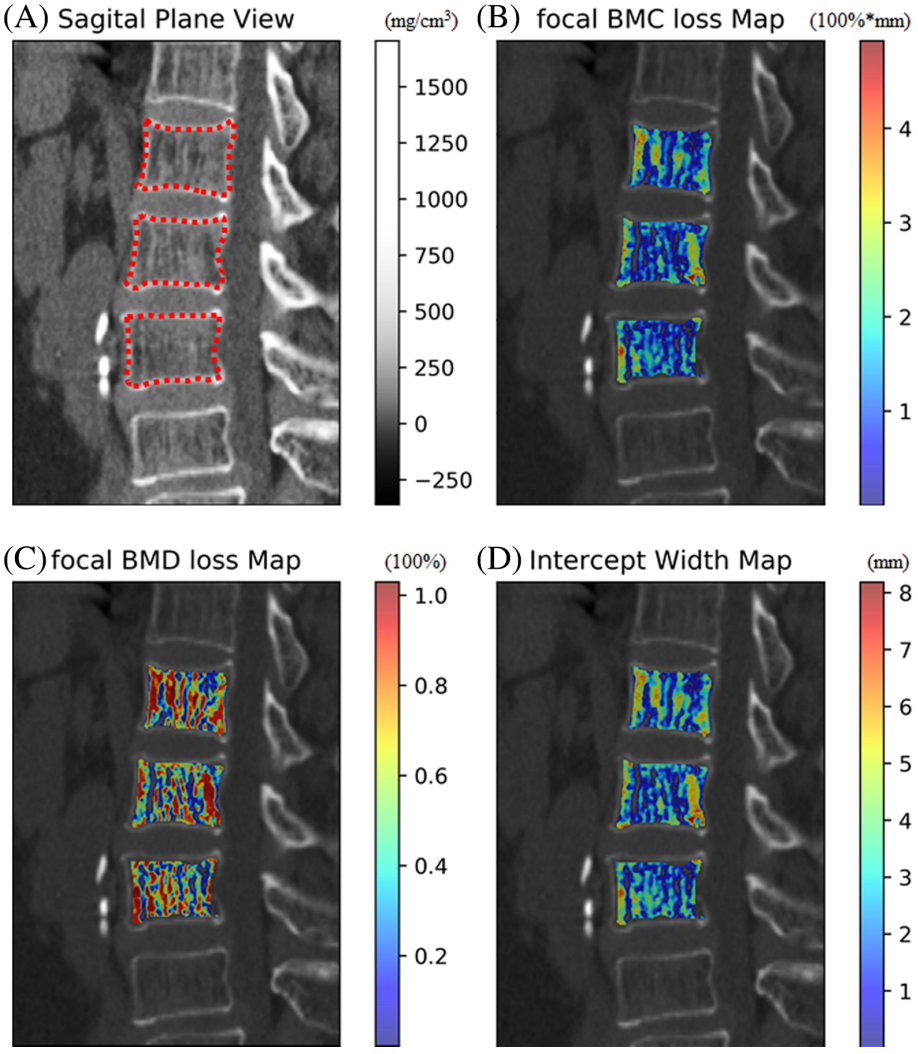

FIGURE 2 Example of the voxel-wise parameter mapping images. (A) The sagittal view of original spinal computed tomography image. (B) The voxel-wise focal bone mineral content loss parameter map. (C) The voxel-wise focal bone mineral density loss parameter map. (D) The voxel-wise intercept width parameter map for red-line contoured vertebrae)

Intel Core i7 CPU environment, the average time-consuming for each calculation was around 2.68 min.

2.4 | Feasibility study

The measurement feasibility, including scan-rescan reproducibly and the measurement correlation with apparent microarchitecture in high-resolution CT, were validated (see text in Appendix A, which demonstrates detailed methods). A flowchart indicating the sample enrollment method for each experiment was present in Appendix B, Figure B1.

2.5 | Statistical analysis

The quantitative variables are described as average ($\bar{x}$) ± standard deviation (*SD*). The differences in quantitative variables, such as age, BMD, and focal osteoporosis defect-related measures between each group were analyzed using one-way ANOVA.

TABLE 1 Reproducibility analysis of each biomarker between two scans

Biomarker	RMSSD	LSC	Bias	LoA	ICC (95% C.I)
Focal BMC loss (mm)	0.011	0.030	0.00	±0.04 (−0.04 to 0.04)	0.97 (0.93–0.99)
Focal BMD loss	0.002	0.007	0.001	±0.008 (−0.07 to 0.09)	0.98 (0.95–0.99)
IncptWidth (mm)	0.016	0.044	0.003	±0.051 (−0.06 to 0.05)	0.96 (0.91–0.98)
BMD (mg/cm^3)	2.61	7.23	−0.1	±8.9 (−9.0 to 8.8)	0.99 (0.98–0.99)

Abbreviations: bias, average of the repeat measurements difference; focal BMC loss, focal bone mineral content loss; focal BMD loss, focal bone mineral density loss; ICC, intraclass correlation coefficient for single measures; IncptWidth, intercept width; LoA, limit of agreement; LSC, least significance change at 95% confidence level; RMSSD, within-subject root mean square of standard deviation.

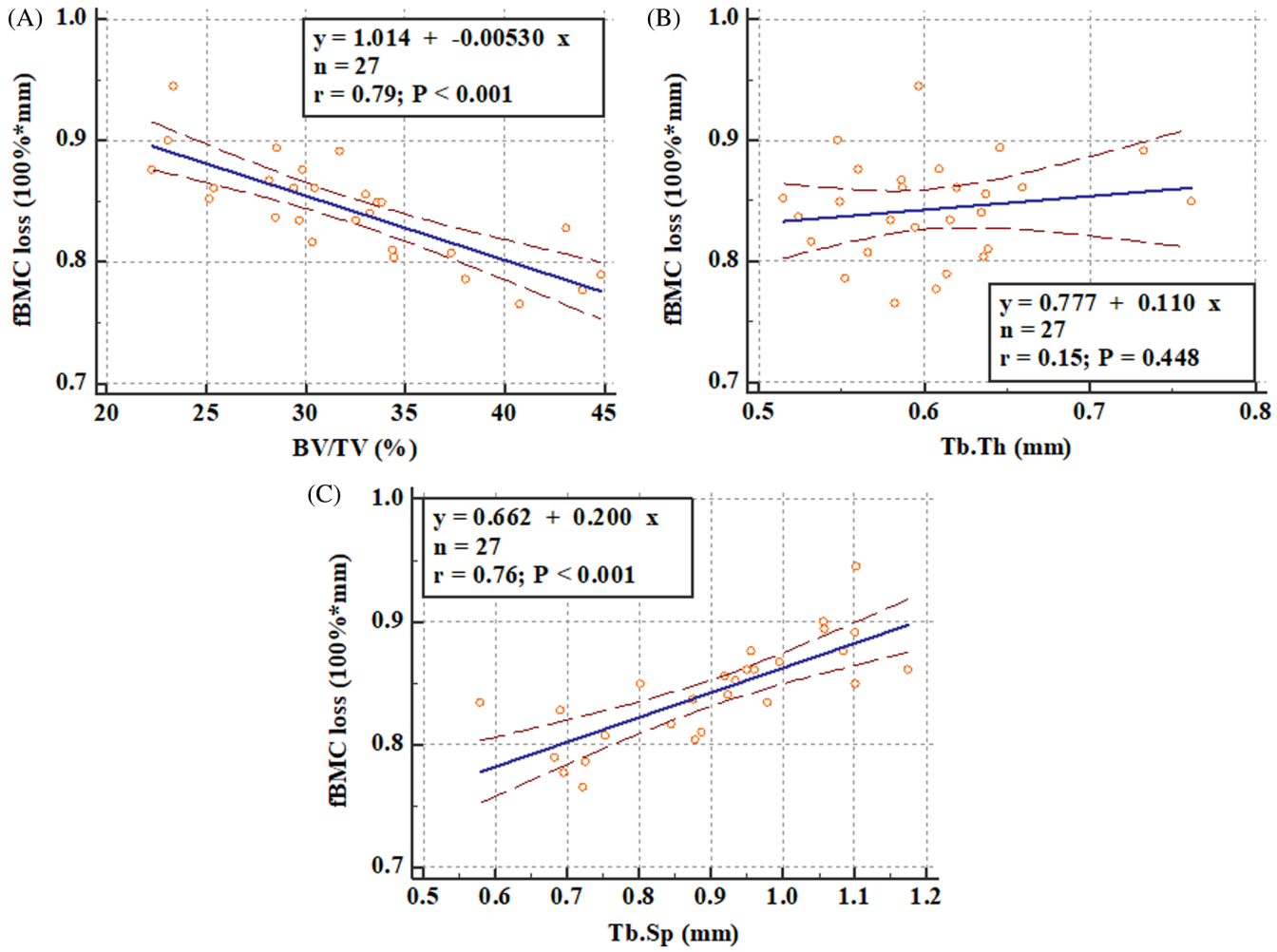

FIGURE 3 Correlation between focal bone mineral content loss and microstructure parameters. (A) Bone volume fraction (BV/TV). (B) Trabecular bone thickness (Tb.Th). (C) Trabecular separation (Tb.Sp)

Pearson correlation coefficient (*r*) was calculated to determine the correlation between focal osteoporosis defect-related measures and BMD. The correlation was classified as: $r > 0.95$, excellent; 0.95–0.85, strong; 0.85–0.70, good; 0.70–0.5, moderate; <0.5, poor.

Conditional logistic regression was used to calculate odds ratios (95% confidence intervals [95% CI]) for the associations of focal osteoporosis defect-related measurements with prevalent vertebral fracture. In these analyses, the fracture or control status was the dependent variable, and focal osteoporosis defect-related measurements were the independent variable. Two regression models were used: the base model had no covariates, while the full model had age and sex as covariates. BMD was also included as a covariate to test the independent association of prevalent fracture with the focal osteoporosis defect-related measurements.

The sample size for independent sample comparison was estimated by power analysis with $\beta = 0.20$ and $\alpha = 0.05$.[23] The sample size for logistic regression was determined by events per variable of 10.[24] As an exploratory analysis, the analyses were also repeated for men and women separately; however, caution should be made when interpreting the results with low statistical power.

Statistical analysis was performed using MedCalc (v19.1, MedCalc Software bv). Significance was set at $P < 0.05$.

3 | RESULTS

3.1 | Scan-rescan reproducibility

The measurement precision (RMSSD), least significance change, and variability of repeat measurements were confirmed in Table 1. The asynchronous BMD measurement showed good precision similar to a previous study.[25] All the measurements showed high reliability with ICC >0.95 (Table 1).

3.2 | Correlation of focal osteoporosis defect-related measurements with the apparent microarchitecture

Focal BMC loss showed good correlation to bone volume fraction ($r = 0.79$, $P < 0.001$), trabecular bone separation ($r = 0.76$,

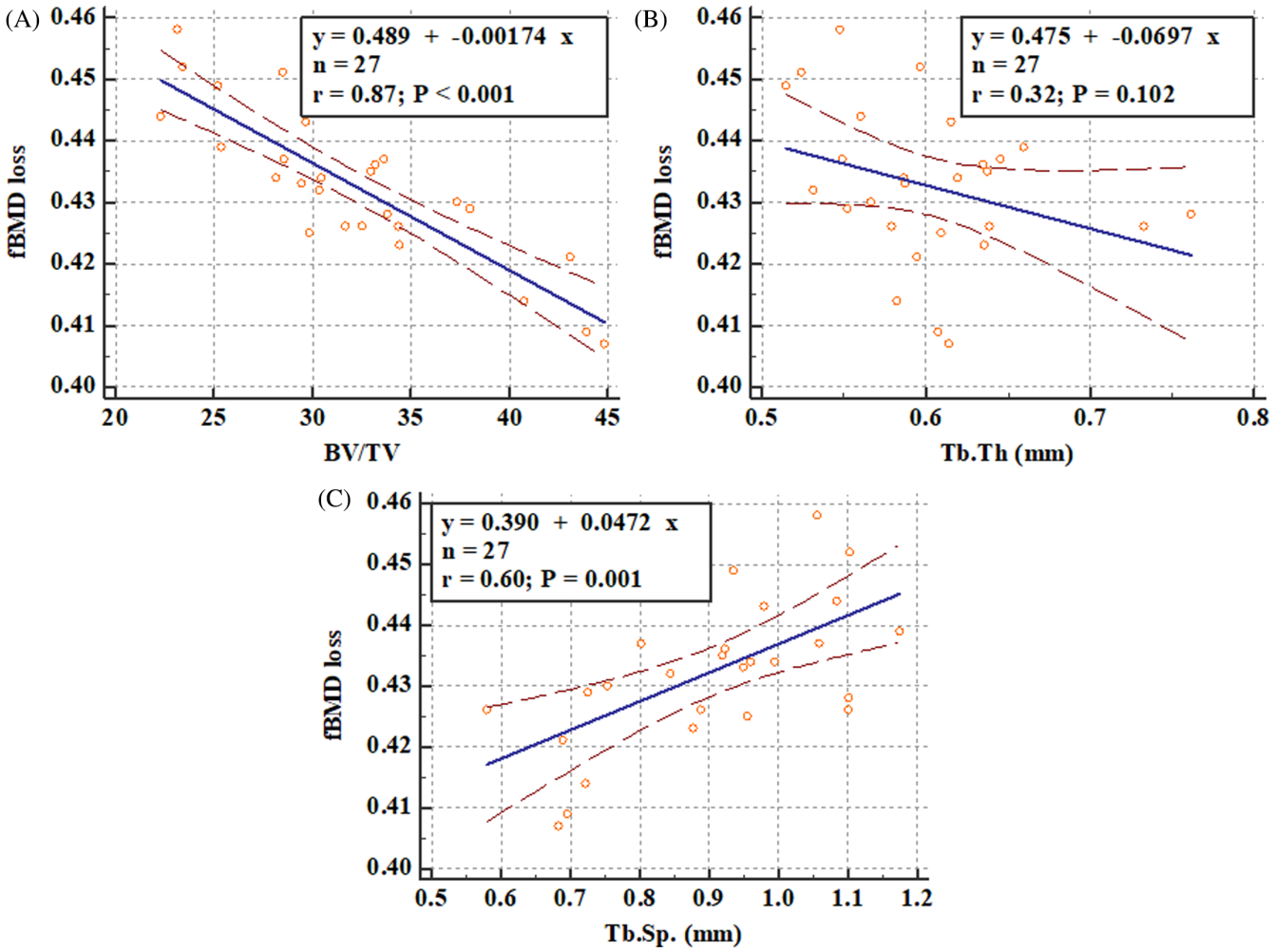

FIGURE 4 Correlation between focal bone mineral density loss and microstructure parameters. (A) Bone volume fraction (BV/TV). (B) Trabecular bone thickness (Tb.Th). (C) Trabecular separation (Tb.Sp)

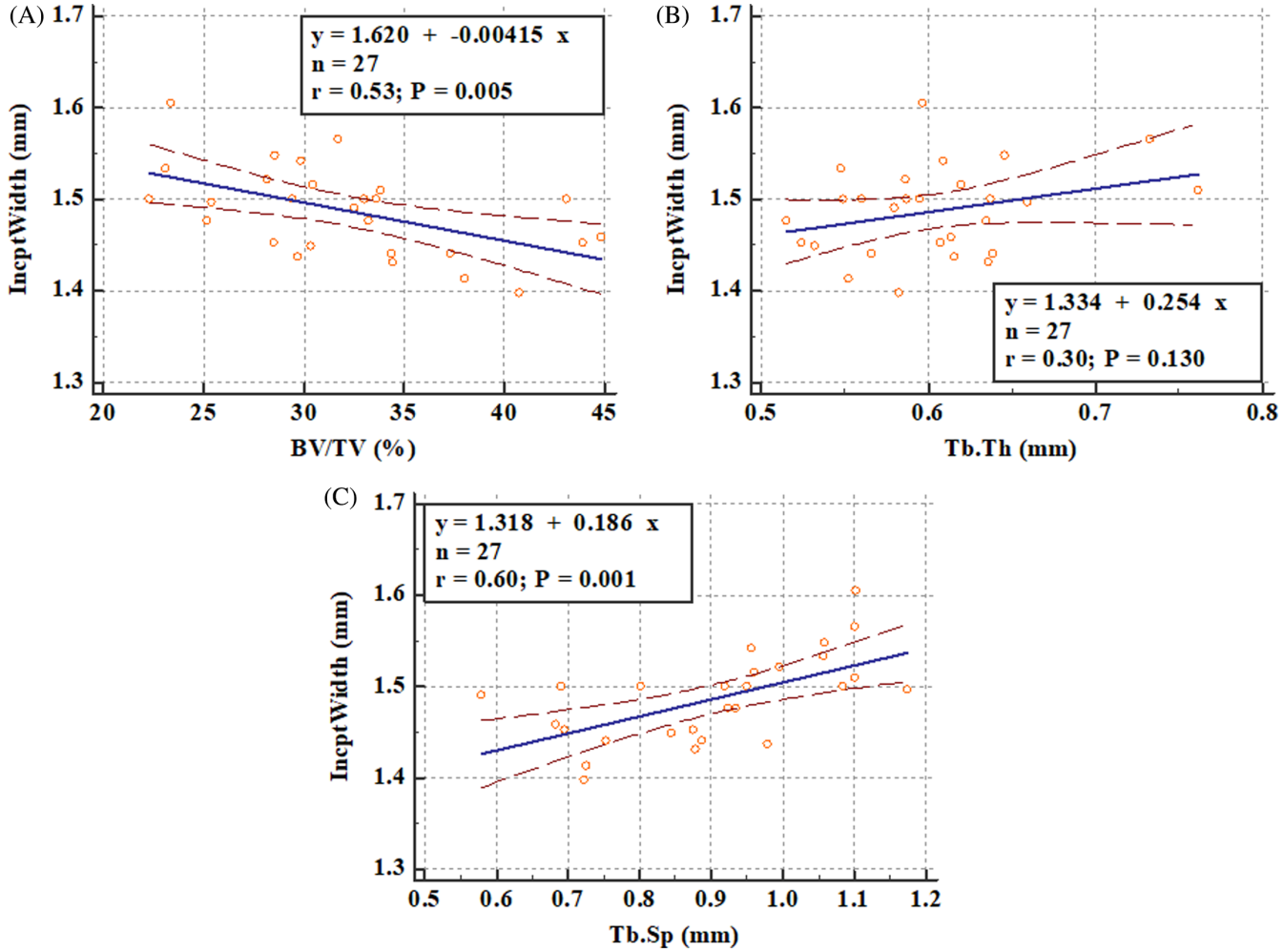

FIGURE 5 Correlation between intercept width and microstructure parameters. (A) Bone volume fraction (BV/TV). (B) Trabecular bone thickness (Tb.Th). (C) Trabecular separation (Tb.Sp)

TABLE 2 Demographic information

	Overall		Women		Men		
	n	Age (year)	*n*	Age (year)	*n*	Age (year)	*P*
Case	91	68.8 ± 8.1	55	68.2 ± 7.2	36	69.8 ± 9.4	0.379
Control	114	67.6 ± 8.4	71	67.1 ± 7.9	43	68.3 ± 8.9	0.469
P	-	0.273	-	0.422		0.478	

Note: Significance was defined as $^*P < 0.10$.

$P < 0.001$) (Figure 3). Focal BMD loss showed a strong correlation to bone volume fraction ($r = 0.87$, $P < 0.001$), but moderate correlation with trabecular bone separation ($r = 0.60$, $P = 0.001$) (Figure 4). With regards to the Intercept Width, moderate correlation with bone volume fraction ($r = 0.53$, $P = 0.005$), trabecular bone separation ($r = 0.60$, $P = 0.001$) was found (Figure 5). Additionally, all measurements showed poor correlations with the trabecular bone thickness.

3.3 | Characteristics of prevalent fracture cases and controls

There was no significant difference in sex and age between the case and control groups (Table 2).

Individuals with prevalent vertebral fracture had higher focal BMD loss and focal BMC loss, but lower BMD. Fracture cases had a higher Intercept Width in women but similar Intercept Width in men subgroup (Table 3).

TABLE 3 Biomarker difference between groups

	Case	Control	*P*
Overall			
Focal BMC loss (100% × mm)	1.03 ± 0.13	0.93 ± 0.11	**<0.001****
Focal BMD loss	0.45 ± 0.03	0.42 ± 0.03	**<0.001****
IncptWidth (mm)	1.95 ± 0.18	1.87 ± 0.18	**0.002****
BMD (mg/cm^3)	77.65 ± 39.86	124.41 ± 71.44	**<0.001****
Women			
Focal BMC loss (100% × mm)	1.02 ± 0.12	0.94 ± 0.12	**<0.001****
Focal BMD loss	0.45 ± 0.02	0.43 ± 0.03	**<0.001****
IncptWidth (mm)	1.92 ± 0.16	1.85 ± 0.18	0.014*
BMD (mg/cm^3)	66.46 ± 33.13	102.64 ± 42.23	**<0.001****
Men			
Focal BMC loss (100% × mm)	1.03 ± 0.16	0.92 ± 0.11	**<0.001****
Focal BMD loss	0.44 ± 0.03	0.41 ± 0.03	**<0.001****
IncptWidth (mm)	1.98 ± 0.21	1.90 ± 0.18	0.057
BMD (mg/cm^3)	94.74 ± 43.54	160.37 ± 92.94	**<0.001****

Note: Data represented as mean ± SD. *P < 0.05, **P < 0.01.
Abbreviations: BMD, bone mineral density; focal BMC loss, focal bone mineral content loss; focal BMD loss, focal bone mineral density loss; IncptWidth, width of the intercept.

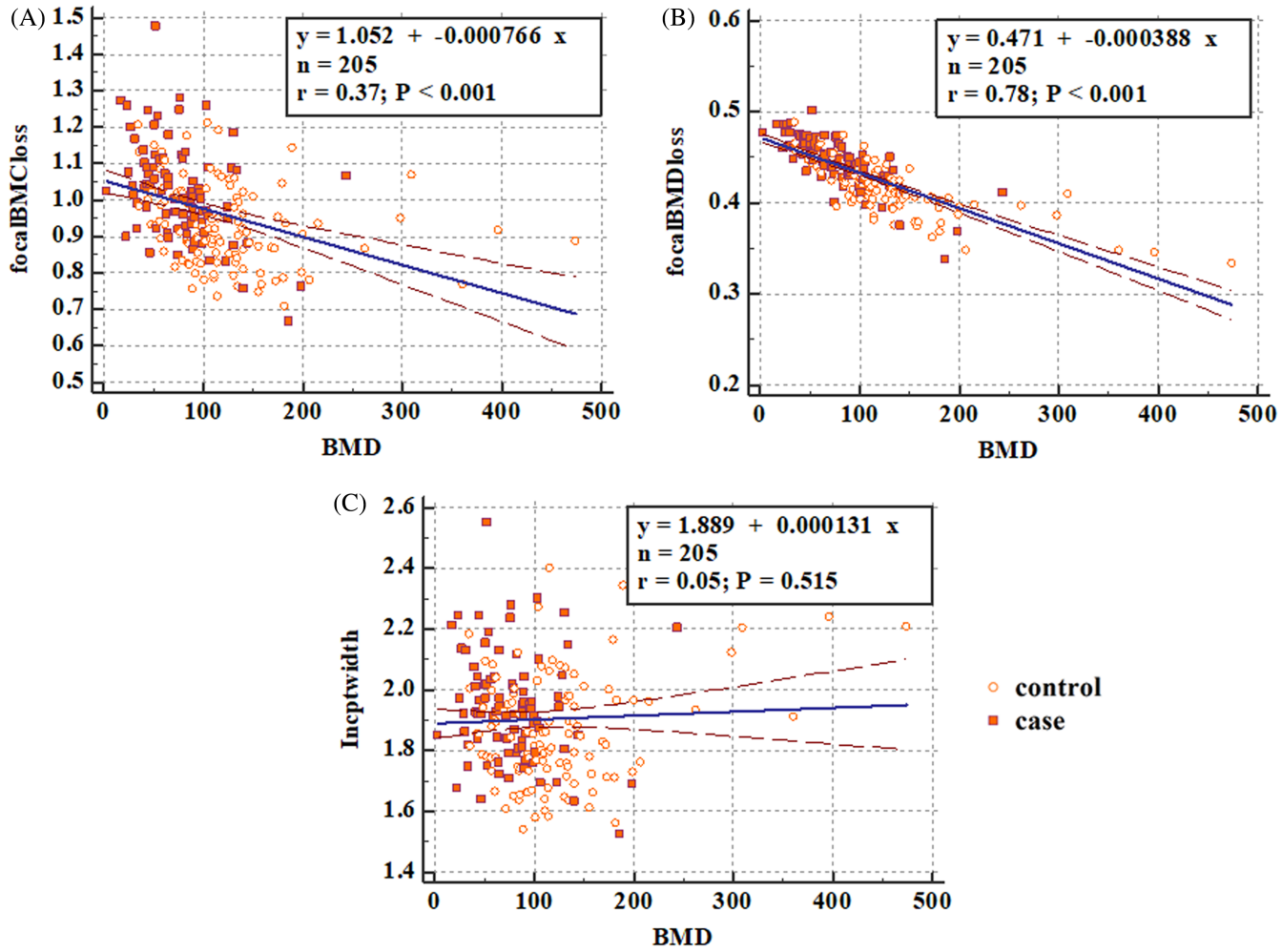

FIGURE 6 The correlation between focal bone mineral content (BMC) loss, focal bone mineral density (BMD) loss, intercept width and Bone Mineral Density. (A) Focal BMC loss. (B) Focal BMD loss. (C) Width of the intercept

TABLE 4 Odds-ratios for the association between prevalent fracture and biomarker values

	Overall		Women		Men	
	Odds ratio[a]	*P*	Odds ratio[a]	*P*	Odds ratio[a]	*P*
Base model (no adjustment)						
Focal BMC loss	2.07 (1.55–2.75)	**<0.001****	2.04 (1.41–2.96)	**<0.001****	2.12 (1.34–3.34)	**0.001****
Intercept width	1.56 (1.17–2.09)	**0.003****	1.62 (1.09–2.40)	**0.017***	1.51 (0.98–2.34)	0.06
BMD	0.24 (0.14–0.42)	**<0.001****	0.15 (0.06–0.35)	**<0.001****	0.24 (0.10–0.59)	**0.002****
Full model (adjusted by age, gender, and BMD)						
Focal BMC loss	1.87 (1.31–2.65)	**<0.001****	1.74 (1.11–2.71)	**0.016***	2.09 (1.15–3.81)	**0.016***
Intercept width	1.80 (1.24–2.61)	**0.002****	1.66 (1.03–2.67)	**0.036***	2.07 (1.09–3.92)	**0.025***

Abbreviations: BMD, bone mineral density; focal BMC loss, focal bone mineral content loss.
Note: *$P < 0.05$, **$P < 0.01$.
[a]Reported as odds per 1SD unit increase in variables; values represented as mean (95% CI), measurements in sex subgroups are reported with adjustment only to age and BMD, with no adjustment to gender.

3.4 | Correlation between focal osteoporosis defect-related measurements and BMD

There was poor correlation between focal BMC loss and BMD ($r = 0.37$, $P < 0.001$). The focal BMD loss was strongly correlated with BMD ($r = 0.78$, $P < 0.001$), while the Intercept Width showed no significant correlation with BMD ($r = 0.05$, $P = 0.515$) (Figure 6).

3.5 | Association between focal osteoporosis defect-related measurements and risk of fracture

The variable of focal BMD loss was excluded in the logistic regression model since the focal BMD loss is linearly correlated with BMD. The focal BMC loss (2.07 [1.55–2.75] overall, 2.04 [1.41–2.96] in women, 2.12 [1.34–3.34] in men, $P < 0.01$) was positively associated with the fracture prevalence in all the base model. Intercept Width showed positive association with the fracture prevalence in overall (1.56 [1.17–2.09], $P = 0.003$) and women base model (1.62 [1.09–2.40], $P = 0.017$), while no significant association with fracture in men subgroup (1.51 [0.98–2.34], $P = 0.06$). Additionally, the decreased BMD was significantly associated with an increased odd of fracture (0.24 [0.14–0.42] overall, 0.15 [0.06–0.35] in women, 0.24 [0.10–0.59] in men, $P < 0.01$).

Moreover, the focal BMC loss was positively associated with fracture prevalence in the full model (1.87 [1.31–2.65] overall, 1.74 [1.11–2.71] in women, 2.09 [1.15–3.81] in men, $P < 0.05$), which indicated the association of focal BMC loss with fracture prevalence was independent to the BMD, age, and gender. Although the Intercept Width was not significantly associated with the prevalent fracture in men base model, a significant positive association was found between Intercept Width and fracture prevalence when the model was adjusted by age and BMD (1.80 [1.24–2.61] overall, 1.66 [1.03–2.67] in women, 2.07 [1.09–3.92] in men, $P < 0.05$) (Table 4).

4 | DISCUSSION

Recently, the CT scans-based opportunistic osteoporotic fracture risk assessment has gained increasing interest and has been efficiently applied in clinical practice.[8] However, the sensitivity of the CT-based bone density to the osteoporotic fracture risk is limited,[26] and it is widely believed that bone quality should also be considered for fracture risk analysis.[5] Recently, the localized BMD distribution has been widely studied and showed a strong association with bone strength and fracture risk.[24,27–29] Moreover, the focal osteoporosis defect observed in routine CT scans, which is a low-resolution manifestation that correlated with focal microarchitecture changes,[3] has shown a positive association with the osteoporosis.[3,6] Nevertheless, most of the previous studies focused on the spatial distribution of the localized bone loss in sub-regions, while merely quantified the actual structural properties of focal osteoporosis defects in routine CT scans.

The analysis of localized structural integrity in clinical medical images has drawn attention for decades.[30–33] However, there is still a shortage of suitable methods for the focal osteoporosis structural integrity quantification in clinical CT scans.[34] Unlike variogram analysis, such as the Trabecular Bone Score (TBS), which is widely applied in DXA devices for structural integrity evaluation,[35–38] CT-based quantification studies drew more attention on apparent microarchitecture estimation. To date, several groups attempted to measure the microarchitecture in multi-detector CT scanners and revealed its association with osteoporosis status.[1,9–12,39] However, previous studies relied upon dedicated high-resolution scanning protocols and did not focus on the focal osteoporosis. The increased radiation exposure and requirement of dedicated protocol made the approaches difficult in routine practice.[40] The surrogate method for focal osteoporosis defect quantification in routine CT scans is still in demand.

The current study developed and validated a new measure, named *focal BMC loss*, to realize the focal osteoporosis defect evaluation in routine CT images. Intuitively, *focal BMC loss* is a comprehensive measurement of the apparent bone void width[41,42] and mineral composition loss. Precisely, the cumulated bone demineralization was

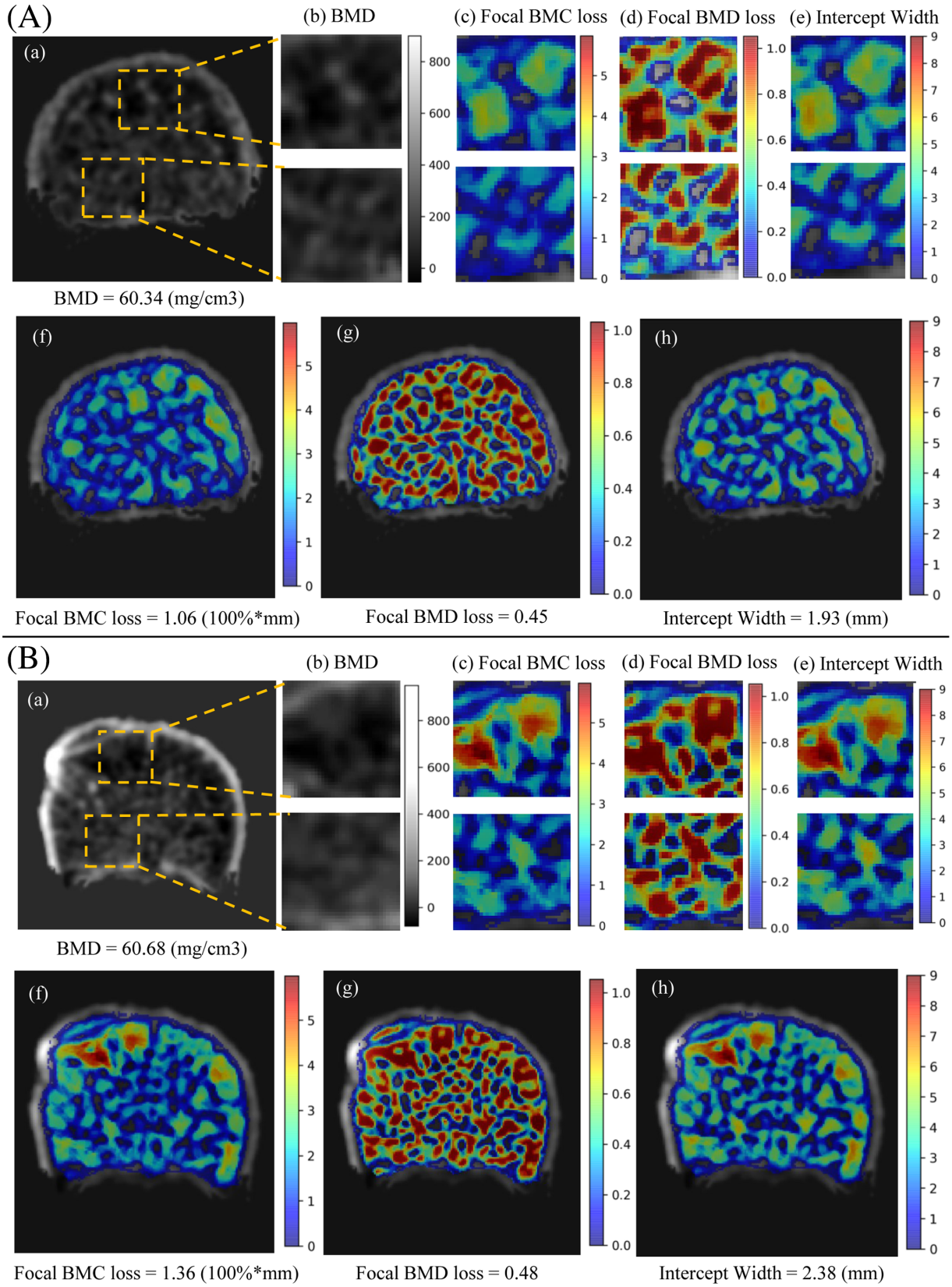

FIGURE 7 Example of the cases with similar bone mineral density but different focal osteoporosis defect measurements. (A and B) Cross-sectional images of the L1 vertebral body from two patients; a: original CT image of the L1 vertebral body; b–e: color maps of bone mineral density and focal osteoporosis defect measurements in sub-regions, figures in the upper row showed larger osteoporosis defect; f–h: color maps and average values of focal osteoporosis defect measurements in the whole cancellous bone region

measured in the focal bone void region; thus, it considers the proportion of demineralization and the bone void space size altogether. Consequently, a higher demineralization fraction weighted by a wider bone void width would lead to a higher *focal BMC loss*, which represents a larger size of focal osteoporosis defect.

In the comparison experiment between routine and high-resolution CT-based microarchitecture measurements, the *focal BMC loss* showed good correlation with both the apparent trabecular bone separation and bone volume fraction in focal regions. In comparison, the *focal BMD loss* and Intercept Width only showed moderate correlation with trabecular bone separation. Since the trabecular separation is a representative property of the localized bone void size,[40,43] it supported that the focal BMC loss at least partially quantified the focal osteoporosis in routine-CT scans.

It should be also noted that the Intercept Width represented the apparent bone void structures in routine CT imaging system, the structures of actual trabecular bone space were resampled by the point spreading function in the low-resolution images.[20] Besides, the intercept width is the half-width distance between local maximum and minimum. It could lead to the case where higher values appear on the void edge rather than the center, where a single large value could exceed multiple medium values. The off-centroid masking may also affect the measurement. Thus, the Intercept Width measurement procedure is different from the micro-CT based trabecular spacing measures, leading to a moderate correlation between Intercept Width and trabecular spacing ($r = 0.6$).

To date, previous studies have reported that the trabecular bone thickness and separation are strongly associated with the osteoporotic fracture risk[1,24,44–47] and biomechanical strength.[45,48] The status of bone marrow tissue measured from the MRI scans was also reported to have a strong correlation with the extent of osteoporosis.[49] The evidence further supported that the bone quality in focal bone void space, reflected by the tissue composition and structural integrity, is related to the bone fragility.

Our study further validated the association of focal bone quality with the prevalence of VCF. The focal BMC loss showed a significant increase in the vertebral body fractured group, with a BMD-independent association with VCF prevalence. In comparison, *focal BMD loss* is highly correlated to the average BMD level, and Intercept Width showed limited association with VCF prevalence. It indicated that the bone mineral content loss in the focal space is an independent factor associated with VCF. One of the reasons is that the average BMD could not reflect the focal defect size, and the difference of bone void width was omitted. In advance, the focal BMC loss measurement helped to discriminate cases with similar integral BMD level but different focal osteoporosis defect size (Figure 7).

Another interesting finding is that in the base model the Odds-ratio of intercept width in men showed no statistical significance. However, in the full model, the intercept width and fracture prevalence showed reversed trend between women and men (Table 2). Since age and sex are not significantly different between groups in the demographic information, the change of prevalence trend in the full model would be majorly caused by the effect of BMD level. These results implicated that the intercept width in men had a stronger association with BMD levels than it in women.

In comparison with the TBS analysis in DEXA, studies showed that the TBS also has moderate correlations with the microstructure parameters in micro-CT ($r^2 = 0.67$ for connectivity density[50]) and poor correlation with the volumetric BMD in spine QCT ($r^2 < 0.5$[51]). Meanwhile, a positive association between TBS and osteoporotic vertebral fracture (hazard ratio = 1.45, 95% I.C.1.32–1.58) was observed.[52]

In the biomechanical aspect, the abnormal stress distribution by focal osteoporosis defects is one of the causes of the positive association between focal BMC loss and fracture risk.[53] Since the voxel-wise BMD are correlated with the elasticity modulus of trabecular bones,[54] lower elasticity modulus with larger bone void space leads to a zone with severer stress shielding. The stress would concentrate on the nearby trabecular bones, leading to higher maximum stress and getting vulnerable to the yield criteria.[55]

Interestingly, we also found that the focal BMC loss was independently increased in the low BMD cases. This result is in agreement with previous histological studies on human cancellous bones.[56,57] In the ex vivo study, microstructure parameters, including trabecular bone separation and trabecular bone thickness, were rapidly changed when the bone volume fraction was <15%,[56] further indicating that the structural integrity would be rapidly decreased in the population with low bone density.

The current study has several limitations. As a retrospective study, the criteria for CT examination were not standardized at the beginning, which may lead to a potential selection bias. Besides, all the measurements were performed in the same CT scanner, the inter-device feasibility was not investigated. Further cohort studies with multiple institutions and larger patient populations are preferred to confirm our findings. Another limitation is that the data from CT scans required more radiation exposure than those from DXEA. Consequently, the included population for those CT-based analyses was further limited by the CT examination indications. The patients without other CT scanning demands or the patients unsuitable for CT scanning may be lost the screening chance. In line with this, the efforts made in CT radiation reduction, such as the low-dose CT would be helpful for the expansion of the CT-based analysis scenario.

In conclusion, *focal BMC loss* in routine CT scans is well correlated to the high-resolution CT-based apparent bone microarchitecture changes, which can be utilized to evaluate the focal osteoporosis defect in addition to the BMD. Furthermore, the clinical evidence supported that the *focal BMC loss* was a BMD-independent risk factor in VCF. It suggests that focal osteoporosis defect is a common manifestation that positively contributed to VCF risk, and can be quantified with routine CT using the *focal BMC loss*.

ACKNOWLEDGMENTS

This work was supported by the Shenzhen Significant Strategy Layout Project (JCYJ 20170413162104773) for Prof. William W. Lu.

CONSENT TO PARTICIPATE

Due to the nature of the retrospective observational study, individual informed consent was waived.

ORCID

Chentian Li https://orcid.org/0000-0002-9362-5952

REFERENCES

1. Ito M, Ikeda K, Nishiguchi M, et al. Multi-detector row CT imaging of vertebral microstructure for evaluation of fracture risk. *J Bone Miner Res*. 2005;*20*(10):1828-1836.
2. Siris ES, Chen YT, Abbott TA, et al. Bone mineral density thresholds for pharmacological intervention to prevent fractures. *Arch Intern Med*. 2004;*164*(10):1108-1112.
3. Poole KES, Skingle L, Gee AH, et al. Focal osteoporosis defects play a key role in hip fracture. *Bone*. 2017;*94*:124-134.
4. Poole KE, Treece GM, Mayhew PM, et al. Cortical thickness mapping to identify focal osteoporosis in patients with hip fracture. *PLoS One*. 2012;*7*(6):e38466.
5. Seeman E, Delmas PD. Bone quality--the material and structural basis of bone strength and fragility. *N Engl J Med*. 2006;*354*(21):2250-2261.
6. Valentinitsch A, Trebeschi S, Alarcon E, et al. Regional analysis of age-related local bone loss in the spine of a healthy population using 3D voxel-based modeling. *Bone*. 2017;*103*:233-240.
7. Osterhoff G, Morgan EF, Shefelbine SJ, Karim L, McNamara LM, Augat P. Bone mechanical properties and changes with osteoporosis. *Injury*. 2016;*47*(Suppl 2):S11-S20.
8. Dagan N, Elnekave E, Barda N, et al. Automated opportunistic osteoporotic fracture risk assessment using computed tomography scans to aid in FRAX underutilization. *Nat Med*. 2020;*26*(1):77-82.
9. Liu Y, Jin D, Li C, et al. A robust algorithm for thickness computation at low resolution and its application to in vivo trabecular bone CT imaging. *IEEE Trans Biomed Eng*. 2014;*61*(7):2057-2069.
10. Saha PK, Wehrli FW. Measurement of trabecular bone thickness in the limited resolution regime of in vivo MRI by fuzzy distance transform. *IEEE Trans Med Imaging*. 2004;*23*(1):53-62.
11. Krebs A, Graeff C, Frieling I, et al. High resolution computed tomography of the vertebrae yields accurate information on trabecular distances if processed by 3D fuzzy segmentation approaches. *Bone*. 2009;*44*(1):145-152.
12. Guha I, Nadeem SA, You C, et al. Deep learning based high-resolution reconstruction of trabecular bone microstructures from low-resolution CT scans using GAN-CIRCLE. *Proc SPIE Int Soc Opt Eng*. 2020;*11317*:113170U.
13. Genant HK, Wu CY, van Kuijk C, Nevitt MC. Vertebral fracture assessment using a semiquantitative technique. *J Bone Miner Res*. 1993;*8*(9):1137-1148.
14. Egger J, Nimsky C, Chen X. Vertebral body segmentation with GrowCut: initial experience, workflow and practical application. *SAGE Open Med*. 2017;*5*:2050312117740984.
15. Fedorov A, Beichel R, Kalpathy-Cramer J, et al. 3D slicer as an image computing platform for the quantitative imaging network. *Magn Reson Imaging*. 2012;*30*(9):1323-1341.
16. Budoff MJ, Malpeso JM, Zeb I, et al. Measurement of phantomless thoracic bone mineral density on coronary artery calcium CT scans acquired with various CT scanner models. *Radiology*. 2013;*267*(3):830-836.
17. Gallardo-Estrella L, Lynch DA, Prokop M, et al. Normalizing computed tomography data reconstructed with different filter kernels: effect on emphysema quantification. *Eur Radiol*. 2016;*26*(2):478-486.
18. Abe K, Katsuragawa S, Sasaki Y, Yanagisawa T. A fully automated adaptive unsharp masking technique in digital chest radiograph. *Invest Radiol*. 1992;*27*(1):64-70.
19. Croucher PI, Garrahan NJ, Compston JE. Assessment of cancellous bone structure: comparison of strut analysis, trabecular bone pattern factor, and marrow space star volume. *J Bone Miner Res*. 1996;*11*(7):955-961.
20. Prevrhal S, Engelke K, Kalender WA. Accuracy limits for the determination of cortical width and density: the influence of object size and CT imaging parameters. *Phys Med Biol*. 1999;*44*(3):751-764.
21. Museyko O, Gerner B, Engelke K. A new method to determine cortical bone thickness in CT images using a hybrid approach of parametric profile representation and local adaptive thresholds: accuracy results. *PLoS One*. 2017;*12*(11):e0187097.
22. Pena JA, Thomsen F, Damm T, et al. Bone-marrow densitometry: assessment of marrow space of human vertebrae by single energy high resolution-quantitative computed tomography. *Med Phys*. 2016;*43*(7):4174.
23. Faul F, Erdfelder E, Lang AG, Buchner A. G*Power 3: a flexible statistical power analysis program for the social, behavioral, and biomedical sciences. *Behav Res Methods*. 2007;*39*(2):175-191.
24. Kaiser J, Allaire B, Fein PM, et al. Heterogeneity and spatial distribution of intravertebral trabecular bone mineral density in the lumbar spine is associated with prevalent vertebral fracture. *J Bone Miner Res*. 2020;*35*(4):641-648.
25. Wang L, Su Y, Wang Q, et al. Validation of asynchronous quantitative bone densitometry of the spine: accuracy, short-term reproducibility, and a comparison with conventional quantitative computed tomography. *Sci Rep*. 2017;*7*(1):6284.
26. Gausden EB, Nwachukwu BU, Schreiber JJ, Lorich DG, Lane JM. Opportunistic use of CT imaging for osteoporosis screening and bone density assessment: a qualitative systematic review. *J Bone Joint Surg Am*. 2017;*99*(18):1580-1590.
27. Gong H, Zhang M, Yeung HY, Qin L. Regional variations in microstructural properties of vertebral trabeculae with aging. *J Bone Miner Metab*. 2005;*23*(2):174-180.
28. Xavier F, Jauregui JJ, Cornish N. Regional variations in shear strength and density of the human thoracic vertebral endplate and trabecular bone. *Int J Spine Surg*. 2017;*11*:7.
29. Antonacci MD, Hanson DS, Leblanc A, Heggeness MH. Regional variation in vertebral bone density and trabecular architecture are influenced by osteoarthritic change and osteoporosis. *Spine (Phila Pa 1976)*. 1997;*22*(20):2393-2401. discussion 2401-2.
30. Pearson RA, Treece GM. Measurement of the bone endocortical region using clinical CT. *Med Image Anal*. 2018;*44*:28-40.
31. Tabor Z. Estimating structural properties of trabecular bone from gray-level low-resolution images. *Med Eng Phys*. 2007;*29*(1):110-119.
32. Varga P, Zysset PK. Sampling sphere orientation distribution: an efficient method to quantify trabecular bone fabric on grayscale images. *Med Image Anal*. 2009;*13*(3):530-541.
33. Majumdar S, Genant HK. Assessment of trabecular structure using high resolution magnetic resonance imaging. *Stud Health Technol Inform*. 1997;*40*:81-96.
34. Loffler MT, Sollmann N, Mei K, et al. X-ray-based quantitative osteoporosis imaging at the spine. *Osteoporos Int*. 2020;*31*(2):233-250.
35. Silva BC, Leslie WD, Resch H, et al. Trabecular bone score: a noninvasive analytical method based upon the DXA image. *J Bone Miner Res*. 2014;*29*(3):518-530.
36. Harvey NC, Gluer CC, Binkley N, et al. Trabecular bone score (TBS) as a new complementary approach for osteoporosis evaluation in clinical practice. *Bone*. 2015;*78*:216-224.
37. Tamaki J, Iki M, Sato Y, et al. Does trabecular bone score (TBS) improve the predictive ability of FRAX((R)) for major osteoporotic fractures according to the Japanese Population-Based Osteoporosis (JPOS) cohort study? *J Bone Miner Metab*. 2019;*37*(1):161-170.
38. Borgen TT, Bjornerem A, Solberg LB, et al. Determinants of trabecular bone score and prevalent vertebral fractures in women with fragility fractures: a cross-sectional sub-study of NoFRACT. *Osteoporos Int*. 2020;*31*(3):505-514.

39. Baum T, Grabeldinger M, Rath C, et al. Trabecular bone structure analysis of the spine using clinical MDCT: can it predict vertebral bone strength? *J Bone Miner Metab*. 2014;*32*(1):56-64.
40. Burghardt AJ, Link TM, Majumdar S. High-resolution computed tomography for clinical imaging of bone microarchitecture. *Clin Orthop Relat Res*. 2011;*469*(8):2179-2193.
41. Whitehouse WJ. The quantitative morphology of anisotropic trabecular bone. *J Microsc*. 1974;*101*(Pt 2):153-168.
42. Moreno R, Borga M, Smedby O. Generalizing the mean intercept length tensor for gray-level images. *Med Phys*. 2012;*39*(7):4599-4612.
43. Bouxsein ML, Boyd SK, Christiansen BA, Guldberg RE, Jepsen KJ, Muller R. Guidelines for assessment of bone microstructure in rodents using micro-computed tomography. *J Bone Miner Res*. 2010;*25*(7):1468-1486.
44. Yeni YN, Poisson LM, Flynn MJ. Heterogeneity of bone mineral density and fatigue failure of human vertebrae. *J Biomech*. 2013;*46*(7):1396-1399.
45. Hulme PA, Boyd SK, Ferguson SJ. Regional variation in vertebral bone morphology and its contribution to vertebral fracture strength. *Bone*. 2007;*41*(6):946-957.
46. Graeff C, Timm W, Nickelsen TN, et al. Monitoring teriparatide-associated changes in vertebral microstructure by high-resolution CT in vivo: results from the EUROFORS study. *J Bone Miner Res*. 2007;*22*(9):1426-1433.
47. Gong H, Zhang M, Qin L, Lee KK, Guo X, Shi SQ. Regional variations in microstructural properties of vertebral trabeculae with structural groups. *Spine (Phila Pa 1976)*. 2006;*31*(1):24-32.
48. Diederichs G, Link TM, Kentenich M, et al. Assessment of trabecular bone structure of the calcaneus using multi-detector CT: correlation with microCT and biomechanical testing. *Bone*. 2009;*44*(5):976-983.
49. Griffith JF. Bone Marrow Changes in Osteoporosis. In Guglielmi G, (Ed.), *Osteoporosis and Bone Densitometry Measurements*; Berlin, Heidelberg: Springer-Verlag; 2013:69-85.
50. Hans D, Barthe N, Boutroy S, Pothuaud L, Winzenrieth R, Krieg MA. Correlations between trabecular bone score, measured using anteroposterior dual-energy X-ray absorptiometry acquisition, and 3-dimensional parameters of bone microarchitecture: an experimental study on human cadaver vertebrae. *J Clin Densitom*. 2011;*14*(3):302-312.
51. Silva BC, Walker MD, Abraham A, et al. Trabecular bone score is associated with volumetric bone density and microarchitecture as assessed by central QCT and HRpQCT in Chinese American and white women. *J Clin Densitom*. 2013;*16*(4):554-561.
52. Hans D, Goertzen AL, Krieg MA, Leslie WD. Bone microarchitecture assessed by TBS predicts osteoporotic fractures independent of bone density: the Manitoba study. *J Bone Miner Res*. 2011;*26*(11):2762-2769.
53. Auger JD, Frings N, Wu Y, Marty AG, Morgan EF. Trabecular architecture and mechanical heterogeneity effects on vertebral body strength. *Curr Osteoporos Rep*. 2020;*18*(6):716-726.
54. Crawford RP, Cann CE, Keaveny TM. Finite element models predict in vitro vertebral body compressive strength better than quantitative computed tomography. *Bone*. 2003;*33*(4):744-750.
55. Wolfram U, Gross T, Pahr DH, Schwiedrzik J, Wilke HJ, Zysset PK. Fabric-based Tsai-Wu yield criteria for vertebral trabecular bone in stress and strain space. *J Mech Behav Biomed Mater*. 2012;*15*:218-228.
56. Parkinson IH, Fazzalari NL. Interrelationships between structural parameters of cancellous bone reveal accelerated structural change at low bone volume. *J Bone Miner Res*. 2003;*18*(12):2200-2205.
57. Tamimi I, Cortes ARG, Sanchez-Siles JM, et al. Composition and characteristics of trabecular bone in osteoporosis and osteoarthritis. *Bone*. 2020;*140*:115558.
58. El Maghraoui A, Zounon AADS, Jroundi I, et al. Reproducibility of bone mineral density measurements using dual X-ray absorptiometry in daily clinical practice. *Osteoporos Int*. 2005;*16*(12):1742-1748.
59. Bland JM, Altman DG. Statistical methods for assessing agreement between two methods of clinical measurement. *Lancet*. 1986;*1*(8476):307-310.
60. Lawson EA, Miller KK, Bredella MA, et al. Hormone predictors of abnormal bone microarchitecture in women with anorexia nervosa. *Bone*. 2010;*46*(2):458-463.
61. Kopp, F.K., K. Holzapfel, T. Baum, et al. Effect of low-dose MDCT and iterative reconstruction on trabecular bone microstructure assessment. Effect of low-dose MDCT and iterative reconstruction on trabecular bone microstructure assessment. *PLoS One*, 2016;*11*(7):e0159903.
62. Munemoto M, Kido A, Sakamoto Y, et al. Analysis of trabecular bone microstructure in osteoporotic femoral heads in human patients: in vivo study using multidetector row computed tomography. *BMC Musculoskelet Disord*. 2016;*17*:13.

How to cite this article: Li, C., Ma, C., Zhuo, X., Li, L., Li, B., Li, S., & Lu, W. W. (2022). Focal osteoporosis defect is associated with vertebral compression fracture prevalence in a bone mineral density-independent manner. *JOR Spine*, *5*(1), e1195. https://doi.org/10.1002/jsp2.1195

APPENDIX A

The materials and methods of feasibility experiments

Experiment 1: Scan-rescan reproducibility

CT image acquisition

The computed tomography (CT) image datasets for the patients who underwent two abdominal CT scans were retrospectively reviewed. The time interval of the two scans was limited within 1 week, to ensure that no change in bone microstructure or density was to be expected during.[58] All the enrolled subjects suffered from the vertebral compression fracture, and the scans were performed in the perioperative period in all cases. Since some of the images were scanned after the percutaneous vertebroplasty, CT image pairs with obvious artifacts were excluded. Finally, 21 pairs ($n = 21$) of CT images were enrolled for the scan-rescan reproducibility analysis.

CT scanning protocol

The routine CT scanning protocol was performed for the same patient. Cases were scanned in spinal view, using Siemens Somatom Definition Flash CT scanner (Siemens). The CT images were scanned with a 1.0 mm scanning thickness. Then the B30s reconstruction kernel and the reconstruction increment of 0.625 mm were applied for the CT image reconstruction. The in-plane spatial resolution of the images was varied from 0.325 to 0.5 mm (average 0.4 mm) due

to the different Field of View (FOV) chosen during scanning. The images were resized using linear interpolation in an in-house python program, and the final apparent spatial resolution was $300 \times 300 \times 300\ \mu m^3$.

Image analysis

The image of the vertebral body region mask was semi-automatically segmented in the Slicer software (v4.8.1)[15] using the grow-cut method. Then the centroid of the vertebral body mask was located. A $1.5 \times 1.5 \times 1.5\ cm^3$ cubic ROI, of which the centroid is as same as the vertebral body centroid position, was selected as the final ROI for microstructure parameters calculation.

The BMD and *focal osteoporosis defect*-related measurement were calculated in the same ROI for each image using an in-house python software. The BMD was calculated based on the average HU value in the ROI and was subsequently converted to the HA-Ca equivalent BMD value based on the asynchronous calibration method. Finally, the measured outcomes from two scans for the same patient were paired for scan-rescan reproducibility analysis.

Statistical analysis

The differences between biomarkers measured in two repeated scans were analyzed by Bland–Altman analysis.[59] The mean of the pairwise differences were reported as bias, and the 95% limits of agreement. The root mean square standard deviation (RMSSD) and least significant change at 95% confidence level (LSC) was also calculated to evaluate short-term measurement precision via the ISCD official precision calculating tool (https://www.iscd.org/resources/calculators/precision-calculator/). The intraclass correlation coefficient was calculated to evaluate the measurement reliability, where the ICC value closer to 1 represents the better measurement reliability.

The quantitative parameters were described as *mean* ± *std*. All the statistical analysis was carried out using MedCalc (v19.1, MedCalc Software bv). The statistical significance was defined as $P < 0.05$.

Experiment 2: Correlation between focal bone defect-related measurements and apparent microstructure parameters

As the high-resolution CT (HR-CT) is the only clinical available in vivo CT imaging method for apparent bone microarchitecture measurement,[40] this study investigated the linear correlation between focal bone loss biomarkers and the HR-CT based apparent microarchitecture parameters. The HR-CT based microarchitecture parameters measurement in clinical CT were reported as an effective way for osteoporotic microarchitecture changes measurement[1,46,60] and showed well correlation to the micro-CT based measurements.[40]

CT image acquisition

For the routine CT and high resolution-CT scanning data collection, the abdominal high-resolution CT image datasets were retrospectively collected from the hospital Picture Archiving and Communication System (PACS) database. Notably, this procedure was independent of the sample collection step mentioned in the main context. The patients with both high-resolution and routine CT scans at the same scanning time were included. For those cases, the routine- and HR-CT images were obtained at the same scanning position, and no further image co-registration was required for comparison. Finally, five patients with both routine- and HR-CT image datasets existed in PACS were included. In each dataset, the thoracic and lumbar vertebral bodies without fracture were selected for analysis. In total, 27 vertebral bodies ($n = 27$) from five patients were included for analysis.

CT scanning protocol

The routine CT scanning protocol was performed for the same patient. Cases were scanned in spinal view, using Siemens Somatom Definition Flash CT scanner (Siemens). The CT images were scanned with a 1.0 mm scanning thickness. Then the B30s reconstruction kernel and the reconstruction increment of 0.625 mm were applied for the CT image reconstruction. The in-plane spatial resolution of the images was varied from 0.325 to 0.5 mm (average 0.4 mm) due to the different FOV chosen during scanning. The images were resized using linear interpolation in an in-house python program, and the final apparent spatial resolution was $300 \times 300 \times 300\ \mu m^3$.

In addition, the high-resolution CT scanning protocol was also available in the same CT scanner. The high-resolution CT scans were performed at 120 kV with automatic current mode, using 0.6 mm scanning thickness and 10 mm FOV. It was leading to an apparent in-plane spatial resolution of $200 \times 200\ \mu m^3$. Furthermore, the images were reconstructed with an increment of 0.2 mm with B70s kernel. The images were resized using linear interpolation in the in-house python program, and the final apparent spatial resolution was $100 \times 100 \times 100\ \mu m^3$.

Image analysis

The HR-CT images were further used for the apparent microstructure parameter calculation. The image of the vertebral body region mask was semi-automatically segmented in the Slicer software[15] using the grow-cut method. Then the centroid of the vertebral body mask was located. A $1.5 \times 1.5 \times 1.5\ cm^3$ cubic ROI, of which the centroid is as same as the vertebral body centroid position, was selected as the final ROI for microstructure parameters calculation.

Binarization of the image was required for the bone microstructure parameter calculation. Based on previous studies,[1,39,61,62] an equivalent bone density level of 200 mg/cm^3 was chosen as the global threshold for binary image generation. Subsequently, the microstructural parameters, such as the bone volume fraction (BV/TV), trabecular bone thickness (Tb.Th), trabecular bone separation (Tb.Sp), were measured using CTAn software (v 1.14.4.1, Bruker Co.).

At the same time, the focal osteoporosis defects biomarkers were calculated from the routine CT images at the same ROI for the same patients using the in-house python software. The corresponding focal osteoporosis defects values in routine CT and apparent microstructure parameters in HR-CT image of the same ROI were paired for correlation analysis.

Statistical analysis

The correlation between the two scans was analyzed using the *Pearson* correlation analysis. Correlation was classified as follows based on correlation coefficient (*r*): >0.95: excellent, 0.95–0.85: strong, 0.85–0.70: good, 0.70–0.5: moderate, <0.5: poor.

The quantitative parameters were described as *mean* ± *std*. All the statistical analysis was carried out using MedCalc (v19.1, MedCalc Software bv). The statistical significance was defined as $P < 0.05$.

APPENDIX B

Flowchart of sample enrollment in each experiment

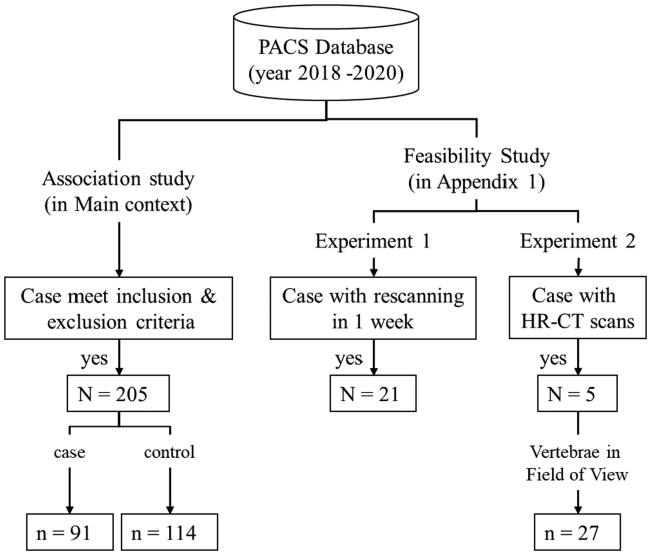

FIGURE B1 Flowchart of sample enrollment in each experiment. For each study, the experiment cases were independently enrolled from the PACS database with different selection criteria